Arc resistance of laser-triggered spark gaps

M. J. Kushner, W. D. Kimura, and S. R. Byron
Spectra Technology, Inc. (formerly Mathematical Sciences Northwest, Inc.), 2755 Northup Way, Bellevue, Washington 98004

(Received 1 April 1985; accepted for publication 16 May 1985)

In the use of spark gaps as switching devices, it is desirable to maximize the power delivered to the load and to minimize the power deposited in the switch; that is, it is desirable for the resistance of the switch to be negligible as compared to the load. The hydrodynamic time scale for expansion of the arc in a spark gap and hence for the reduction in its resistance to a small value is tens to hundreds of nanoseconds. Therefore, with current pulses of duration of a few hundred nanoseconds or less, the resistance of the spark gap may be a significant fraction of that of the load. In this paper, we report on measurements that determine the resistance of the arc in a fully diagnosed laser-triggered spark gap. The spark gap switches a 100-ns, 1.5-Ω waterline into a 1.5-Ω load resistor. A capacitive voltage divider housed within the switch enclosure measures the voltage drop across the switch, a current-viewing resistor measures the current, and an interferometer measures the diameter of the plasma column, a value required to calculate its inductance. The resistance of the arc is found to remain in excess of 0.1–0.2 Ω for the duration of the current pulse for a variety of switch gas mixtures. The resistance decreases with increasing charging voltage on the waterline at the time of triggering and decreases with decreasing average molecular weight of the gas mixture in which the arc is sustained.

I. INTRODUCTION

Spark gaps are commonly used devices in applications where high voltages and currents must be economically switched in short times. The holdoff voltages required for these applications range from tens of kilovolts to a few megavolts, and conduction currents range from tens of kiloamps to a few mega-amps. In many instances it is desirable that the switching spark gap operates with a minimum of jitter, that the spark gap operates over a wide range of holdoff voltages, and that the resistance of the spark gap during conduction is negligible compared to the load in order to minimize the power loss associated with the switching device. With the development of laser preionization triggering of spark gaps,[1–6] the jitter of spark gaps has been dramatically reduced and the voltage operating range of the devices has been greatly increased.[1–3] The resistive loss of laser-triggered spark gaps, though, until now has not been carefully investigated and is the subject of this paper.

Although our paper will address the resistance of laser-triggered spark gaps operating through a *single* channel, the discussion which follows is also applicable to other types of spark gaps operating through a *single* channel. The conditions of our experimental study, however, are in a parameter space not previously addressed in detail. The duration of our current pulse ($\approx$ 100 ns) is shorter, and the current density in our spark column ($\approx$ 2 MA/cm^2) is higher than the typical self-breaking spark columns previously studied.[7] In addition, the number of channels through which those spark columns operated is not known and the selection of gases differs, thereby complicating direct comparison. Some limited comparison, though, can be made to previous work by examining the properties of those spark columns during the first hundred nanoseconds of their current pulses.

Early during the conduction phase of a spark gap, whether it be laser preionization triggered, electrically triggered, or self-breaking, the resistance of the arc between the spark gap electrodes is large compared to the load. During the first tens to hundreds of nanoseconds after triggering (or self-break), the plasma arc expands from an initial diameter[8] of $\approx 50\,\mu$m to a diameter greater than a millimeter. As the arc expands and increases its cross-section area, the resistance of the arc decreases proportionally. The time required to reduce the resistance of the arc from an initially large value (many tens of ohms) to a resistance small compared to the load ($\leqslant 0.1\,\Omega$) is, therefore, dictated by the hydrodynamic time scale, that is, the time required for the arc to hydrodynamically expand to sufficiently large radius.[8–11] If the duration of the current pulse delivered to the load is comparable to the time required for the arc to expand, resistive losses in the switch will be non-negligible.

In most applications of spark gaps as switches, the primary interest is logically with the voltage drop across the load and not with the switch. Therefore, estimates of the resistance of (and, hence, losses associated with) the spark gap are many times based on the difference between stored energy and energy delivered to the load. Even when attention is directed to the spark gap, the measurement of the resistance of the arc is difficult due to the difficulty in measuring the resistive component of the voltage drop across the arc. This measurement is complicated by the fact that the dynamic range of the voltage that must be measured is large ($>$ 100 kV to $<$ 1 kV) and that a major fraction of the measured voltage between the spark-gap electrodes is attributable to inductive effects. The source of this inductance is in the fixed geometry of the switch, in the electrical connections to the voltage measuring device, and in the plasma arc itself. To obtain a measure of the last component of inductance, the time history of the size of the arc must be known.

In this paper, we report on the results of a study of arc resistance in a fully diagnosed laser-triggered spark gap op-

 0021-8979/85/171744-08$02.40

erating through a single channel for current pulses ≈ 100 ns in duration. Results for the resistances of arcs through a selection of gases having a wide range of molecular weights and for voltages from 0.1 to 1.2 times the dc self-break value are reported. We find that the resistance of the arc during the time scale of interest remains in excess of 0.1–0.2 Ω and that the voltage drop across the arc remains in excess of a few kilovolts. The resistance of the arcs can be correlated with the average molecular weight of the gas mixture; it is roughly inversely proportional to the average molecular weight, a condition that supports hydrodynamic expansion of the arc channel as being the mechanism by which the resistance of the arc is reduced. In Sec. II, the experimental apparatus and data-reduction technique are discussed. In Sec. III, results for the resistances of a variety of spark columns are presented. Concluding remarks are given in Sec. IV.

II. EXPERIMENTAL APPARATUS AND DATA-REDUCTION TECHNIQUE

The experimental system, described in detail elsewhere,[8] is shown in Fig. 1. The apparatus consists of a 1.5-Ω, 100-ns waterline that is pulsed charged in 1.8 μs by a two-stage Marx bank to a voltage between 40 and 100 kV. Attached to the waterline is a chamber that houses a laser-triggered spark gap. The spark gap consists of two hemispherical copper electrodes placed 1.2 cm apart, each having a 1-mm-diam hole through their centers. The preionization laser beam enters the electrode gap through the hole in the anode, is focused at a point midway between the electrodes, and passes through the hole in the cathode without striking either of the electrodes. This method of triggering produces a spark channel which is very reproducible, axisymmetric, and is accurately controlled both temporally (jitter < 4 ns) and spatially (jitter $< 10\,\mu$m).

The low jitter and the temporal and spatial reproducibility of the spark columns obtained by use of laser preionization triggering permits the spark column to be studied with a pulsed laser interferometer. Access for optical diagnostics is provided by two sets of ports located orthogonally around the spark-gap housing. The laser interferometer, also described in Ref. 8, provides a measure of the diameter of the current-carrying portion of the spark column with a time resolution of < 5 ns. This diameter is used to calculate the inductance of the spark column in the manner described below. A typical interferogram of the arc in a laser-triggered spark gap obtained with our laser interferometer is shown in Fig. 2. The outermost fringe shift is due to shock-wave compression of the ambient gas. The inner fringe jump is caused by an abrupt rise in ionization of the gas. See Ref. 8 for a more detailed description of the later interferometer measurements.

In order to calculate the resistance of the arc in a spark column, the voltage drop across and current through the arc channel must be accurately known. The current through the spark column is measured with a current-viewing resistor (CVR). The CVR consists of an Inconel foil surrounding the spark-gap chamber. The CVR completes the current return path between the switch and load resistor, and the waterline.

The voltage drop between the spark-gap electrodes is measured with a capacitive voltage divider (CVD) specifically designed for use in this spark-gap chamber. The CVD, shown schematically in Fig. 3, will be only briefly described here since details of the design and construction of the device appear elsewhere.[12,13] The CVD is annular in shape and is mounted within the spark-gap chamber. The capacitors C_1 and C_2 consist of three flat rings which are centered on the spark column axis and oriented perpendicular to the axis. C_1 corresponds to the capacitance between rings 1 and 2 while the capacitance between rings 2 and 3 corresponds to C_2. The solid dielectric between rings 1 and 2 is polyethylene, whereas the dielectric between rings 2 and 3 is a single layer of 0.025-mm-thick Kapton. The upper and lower plates of capacitors C_1 and C_2 are directly connected to the anode and cathode electrodes, respectively. This geometry minimizes the inductance of the CVD and minimizes the inductive

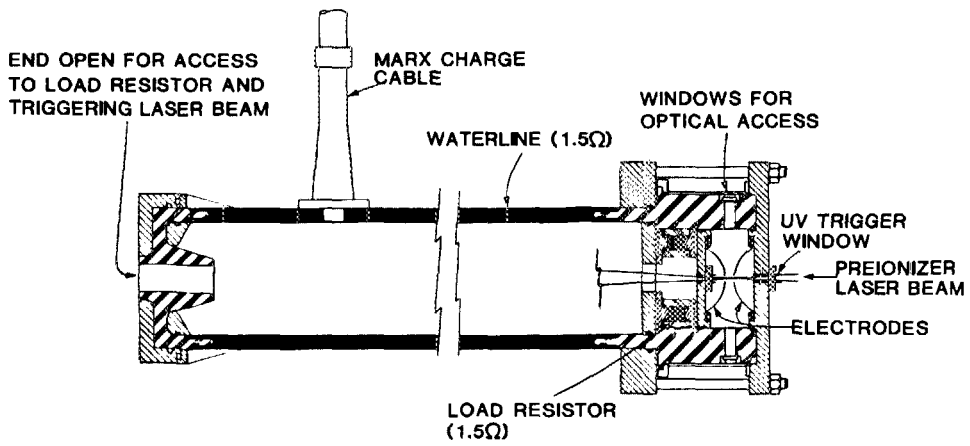

FIG. 1. Schematic of experimental apparatus. The 1.5-Ω, 100-ns water pulse-forming line is terminated by a liquid copper sulfate load resistor and switched by the laser-preionization-triggered spark gap. The preionization laser enters and leaves the interelectrode gap coaxially through 1-mm holes in each eletrode. The minimum electrode spacing is 1.2 cm. The spark-gap chamber sits within the one leg of a Mach-Zender interferometer. The probe beam for the interferometer interrogates the arc perpendicular to the axis of symmetry. The probe laser enters and leaves the spark-gap chamber through the optical access windows indicated.

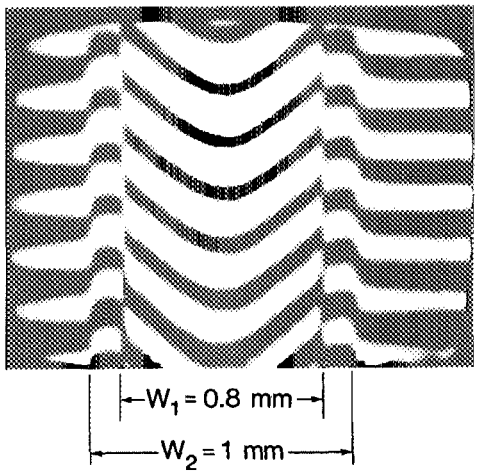

FIG. 2. Typical interferogram of the arc in a laser preionization triggered spark gap taken 40 ns after breakdown. The gas mixture is 2 atm of Xe/H_2 : 0.01/0.99. The voltage on the waterline at the time of triggering is approximately 40 kV. The time resolution of the interferogram is <5 ns. The diameter of the laser preionized region at $t=0$ is $\approx 50\,\mu$m. The width W_1 indicates the diameter of the current carrying core of the arc. The width W_2 indicates the total diameter of the arc, including a high-density, largely neutral shell surrounding the ionized core.

component of the voltage measured by the CVD. The rise time of the probe is estimated to be less than 1 ns.

The values of C_1, C_2, R_1, and R_2 were chosen to ensure that the error in the voltage measurement due to voltage decay across C_2 during the current pulse (≈ 100 ns) is less than 1%. The time required to charge the waterline (1.8 μs), though, is not short compared to the RC time constant for the decay of the voltage on C_2 ($RC = 9.8\,\mu$s). Therefore, the voltage indicated by the probe, V_0, at the time of triggering is less than the charging voltage on the waterline, V_l. The values of capacitors C_1 and C_2 were determined experimentally (see below) and the time rate of change of voltage on the waterline during charging is accurately known by experimental measurements; therefore, this effect can be corrected for by analysis of the equivalent circuit for the CVD[12,13]:

$$V_0(t) = V_0(0)\exp\left(-\frac{t}{RC}\right) + \frac{R_2C_1}{RC}\exp\left(-\frac{t}{RC}\right) \times \int_0^t \frac{dV_l(t')}{dt'}\exp\left(\frac{t'}{RC}\right)dt', \quad (1)$$

where $C = C_1 + C_2$ and $R = R_1 + R_2$. For our conditions, the voltage indicated by the CVD at the time of laser triggering of the spark gap is 0.91 V_l. During the current pulse, the change in voltage from the initial value as indicated by the probe is used without further correction. Typical current and voltage waveforms obtained with our probes are shown in Fig. 4.

For $V_0(t)$, as calculated from Eq. (1), to be accurate the values of R_1, R_2, C_1, and C_2 must be precisely known. The resistors R_1 and R_2 are discrete components, enabling their values to be accurately measured using conventional resistance meters. The capacitance C_2 was measured *in situ* using a vector impedance bridge, yielding a value of 5.0 nF. Due to geometrical limitations, a direct measurement of C_1 could not be made. The capacitance of C_1 was obtained by measuring the total attenuation of the probe for a known voltage input and using the known values of R_1, R_2, and C_2 to calculate C_1 from Eq. (1). This was done using the voltage across the spark gap during the charging cycle of the pulse-forming line (PFL). During the slow (1.8-μs) pulse charging of the PFL, the spark-gap voltage can be reliably measured using a resistive divider probe, thereby providing a reference value. Using this method, we obtained a value of 11.5 pF for C_1.

As an additional check of the capacitance values, the voltage decay time constant of the output of CVD was measured. Since R_1 and R_2 are accurately known and the attenuation factor is known, the values of C_1 and C_2 can be obtained from Eq. (1). Using this method, C_1 and C_2 were found to be 10.66 and 4.35 nF, respectively. Since the duration of the current pulse (≈ 100 ns) is small compared to the RC time constant of the CVD (9.8 μs) Eq. (1) can be approximated during the current pulse as $V_0(t) = (R_2C_1/RC)V_s(t)$, where $V_s(t)$ is the total voltage drop across the spark. The uncertainty in our voltage measurements is therefore the uncertainty in the derived attenuation factor C_1/C. From our two

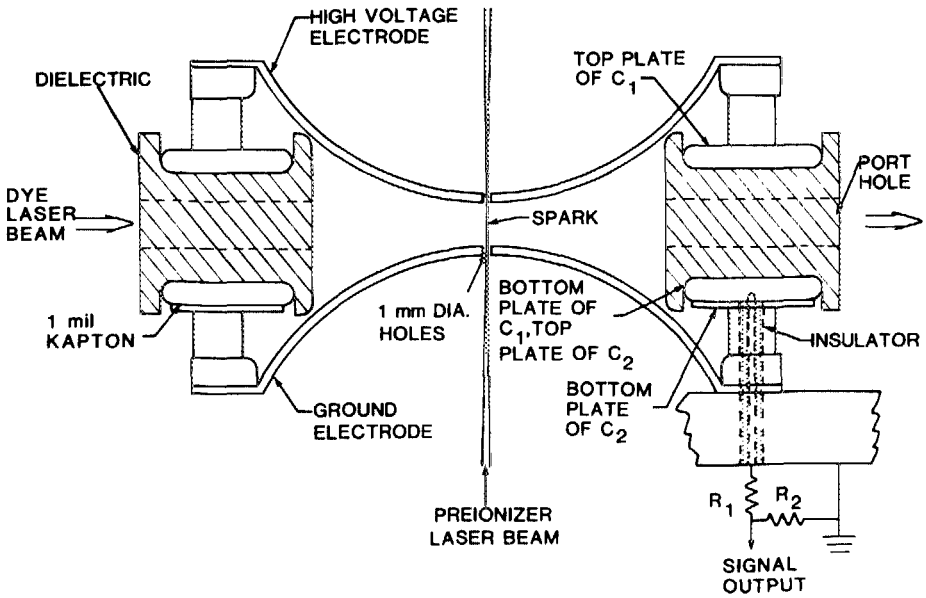

FIG. 3. Schematic of the capacitive voltage divider (CVD) voltage probe showing the mounting configuration around the spark gap electrodes. The CVD is annular. The figure is a section taken through the center of the electrodes. The electrode separation is 1.2 cm.

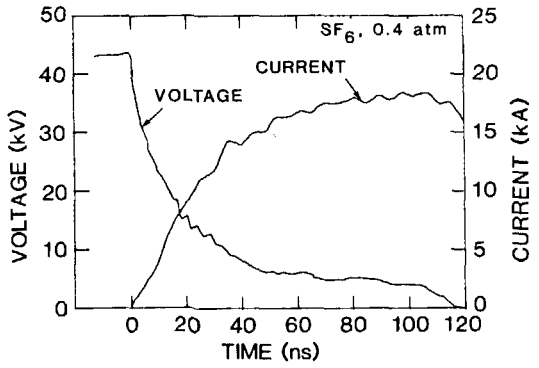

FIG. 4. Typical voltage and current traces taken with the current-viewing resistor and capacitive voltage divider (CVD). The gas is 0.4 atm of SF_6. The voltage scale has been corrected for droop in the CVD that occurs during the 1.8-μs charging time.

determinations of this ratio, the uncertainty in our voltage measurements is $\pm$ 3.2%.

We desire to obtain the time-dependent resistance of the arc in the spark gap, $R_s(t)$. This quantity is simply $V_r(t)/I(t)$, where $V_r(t)$ is the resistive voltage drop across the arc and $I(t)$ is the total current. However, the voltage measured by the CVD is

$$V_0(t) = I(t)R_s(t) + [L_s(t) + L_f]\frac{dI(t)}{dt} + I(t)\frac{dL_s(t)}{dt}, \quad (2)$$

where $L_s(t)$ is the time-varying inductance of the spark column and L_f is a constant inductance value attributable to the geometry of the electrodes ($\approx$5 nH). For our conditions, the last term in Eq. (2) is small and can be neglected. To obtain $R_s(t)$ from Eq. (2), the measured voltage and current waveforms (as they appear in Fig. 4) are digitized and entered as inputs to a computer program. In the program, the current waveform is numerically differentiated to provide $dI(t)/dt$. The last remaining quantity required to solve for $R_s(t)$ is the spark-channel inductance $L_s(t)$. This value is obtained from the time history of the spark-channel radius as measured from laser interferograms taken coincidently with the voltage and current measurements. Assuming current flows uniformly through the spark column, the value of $L_s(t)$ is given approximately by

$$L_s(t) \cong l\frac{\mu_0}{2\pi}\ln\left(\frac{r_c}{r_s(t)}\right), \quad (3)$$

where l is the length of the spark column, r_c is the radius of the current return path ($\approx$14 cm), and $r_s(t)$ is the radius of the spark channel obtained from the interferograms. With this value of $L_s(t)$, it is posible to solve for the spark-channel resistance $R_s(t)$ from Eq. (2). It is this value we refer to in the remainder of this paper.

III. RESULTS FOR THE RESISTANCE OF ARCS IN LASER-PREIONIZATION-TRIGGERED SPARK GAPS

A. Laser-preionization-triggered sparks in SF_6

In the discussion that follows, we reference the charging voltage of the waterline at the instant of laser triggering, V_l, to the dc self-break value, V_{SB}. This value, $F_{SB} = V_l/V_{SB}$, often appears as an independent parameter in measurements of spark-breakdown characteristics. The self-break voltage was measured under quasi-dc conditions with an identical set of electrodes to those used in the laser-triggered spark gap. For our conditions, V_{SB} is a nearly linear function of gas pressure over the pressure range of 0.25–2.0 atm. The measured coefficients of proportionality for the gas mixtures discussed in this paper are given in Table I. Although our measurements were made with a constant electrode spacing, we have expressed the dc self-breakdown coefficient as being normalized per unit electrode spacing distance. Since our waterline is pulse charged (charging time 1.8 μs), it is possible for the spark gap to hold off a voltage greater than the dc self-break value before laser triggering occurs. When measured on a pulsed basis on the water line, the pulsed self-break voltage was found to be approximately 20% greater than the dc value. Recall that all of the experimental data we present is for a constant current-pulse duration (100 ns) and therefore an arc operating at a higher voltage (i.e., higher F_{SB} at constant pressure) also operates at a higher current. Scaling laws we present based on experimental data are only valid for current pulse durations of approximately 100 ns.

Typical plots of arc resistance as a function of time after laser triggering are shown in Fig. 5 for SF_6 at three values of F_{SB}. Values are plotted for only the first 100 ns of the current pulse; that is, for the first PFL transit time. These plots have been digitally filtered to remove small oscillations in the resistance that occur after 50 ns. Recall that these plots are for a spark column operating through a *single* channel. Arcs operating through more than one channel may have different characteristics than those shown here. In multichannel arcs, current is shared between the channels and the resistance of the arc is the effective resistance of many arcs in parallel. Note that the resistance of the arcs decreases rapidly during the early channel-expansion phase and reaches a plateau value. The resistance decreases only marginally once this plateau value has been reached. As F_{SB} increases, the time at which the plateau resistance is reached decreases, and the value of that resistance also decreases. The plateau resistance of the arcs decreases with increasing values of F_{SB},

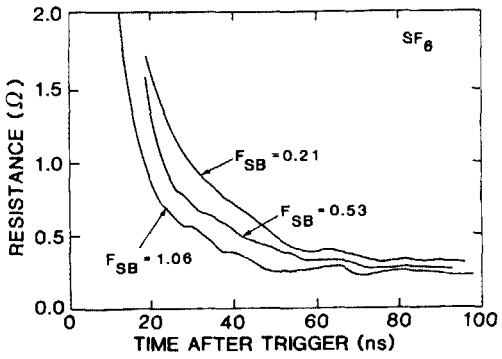

FIG. 5. Arc resistance as a function of time after laser preionization triggering for sparks in SF_6. These resistances are for three values of $F_{SB} = V_l/V_{SB}$ (fraction of dc self-break voltage on the waterline at the time of triggering). This data were obtained by deconvoluting experimental voltage and current traces using the arc diameter measured by laser interferometry.

as shown in Fig. 6. This trend will be discussed in more detail below.

During the first 100 ns of the current pulse, the diameter of the arc increases nearly linearly with time, and the rate of growth in the diameter of the arc increases with increasing F_{SB}. For SF_6, the rate of expansion, ρ_e, is plotted in Fig. 7, and is given approximately by

$$\rho_e = 3.2 + 20.8F_{SB} - 8.55F_{SB}^2 \text{ mm } \mu s^{-1},$$
$$0.1 < F_{SB} < 1.2. \quad (4)$$

In spite of the continued increase in the diameter of the arc at times greater than 50 ns, the resistance of the arc nevertheless plateaus to a relatively constant value. This effect can be qualitatively understood by the following model.

Assume the arc is in local thermodynamic equilibrium (LTE) and that the degree of ionization of the arc has exceeded the limit required to reach Spitzer conductivity (1–10% ionization is sufficient). In this limit, the electrical conductivity of the plasma, $\sigma(t)$, is proportional to $[T_e(t)]^{3/2}$, where $T_e(t)$ is the time-dependent electron temperature.[14] For LTE conditions, $T_e(t) = T(t)$, where T is the gas temperature. In addition, we stipulate that $T(t)$ is proportional to the instantaneous heating rate per atom, $[j(t)]^2/[N(t)\sigma(t)]$, where j is the average current density and N is the atom number density. If no mass is entrained into the arc and the arc grows predominantly by hydrodynamic expansion of the ionized core (also known as the snowplow model), then $N(t) \propto A_0P_0/A(t)$, where P_0 is the initial gas pressure and $A(t)$ is the cross-section area of the arc, $A(t) = \pi(\rho_e t)^2/4$. We assumed that the initial cross-section area of the arc $A_0 \propto F_{SB}^{\alpha}$. This assumption will be discussed below. With these assumptions, we have for the gas temperature T and the arc resistance R,

$$T \propto \frac{j^2}{N\sigma} \propto \left(\frac{I}{A}\right)^2 \frac{A}{T^{3/2}P_0F_{SB}^{\alpha}} \rightarrow T \propto \left(\frac{I^4}{P_0^2(F_{SB}^{\alpha})^2A^2}\right)^{1/5}, \quad (5)$$

$$R = \frac{L}{\sigma A} \propto \frac{1}{T^{3/2}A} \propto \left(\frac{P_0^3(F_{SB}^{\alpha})^3}{A^2I^6}\right)^{1/5}, \quad (6)$$

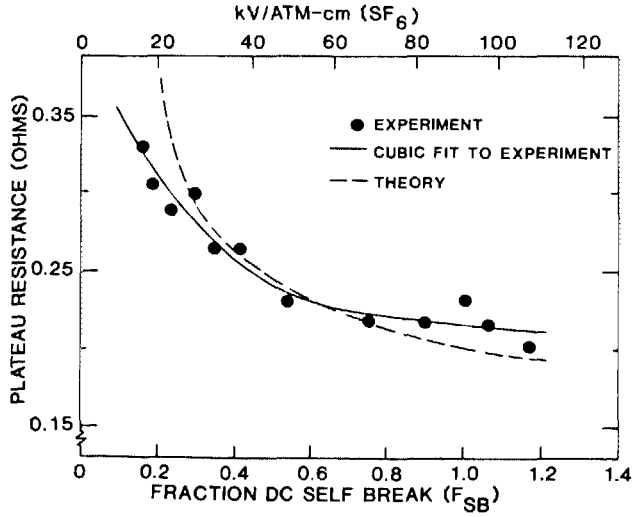

FIG. 6. Plateau arc resistance for SF_6 as a function of the fraction of dc self-break that the waterline is charged to at the time of laser preionization triggering. The solid line is a cubic fit to the experimental points and the dashed line is the result of our simple model [see text and Eq. (6)].

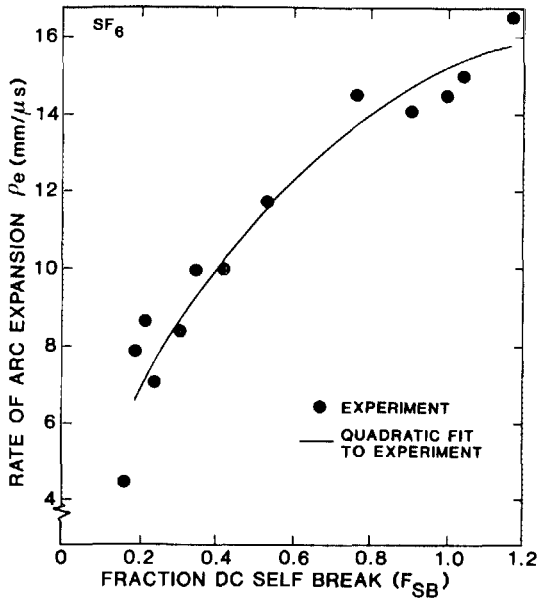

FIG. 7. Rate of expansion in the diameter of the arc in SF_6 as a function of the fraction of dc self-break that the waterline is charged to at the time of laser triggering. The arc expands nearly linear in time with the coefficient indicated in the figure. The experimental points were obtained from analysis of laser interferograms of the spark column. The solid line is a quadratic fit to the experimental data.

where L is the length of the plasma column. We see that as the arc expands, the resistance of the arc decreases simply as a result of the increase in the cross-section area of the arc. But as the cross-section area increases, the temperature of the arc decreases as a result of a lower volumetric heating rate. Therefore, the resistance of the arc is a convolution of these two opposing effects. The average electical conductivity of the arc may, in fact, decrease simultaneously to the total resistance decreasing provided that the area of the arc increases at a sufficiently high rate. The result of these opposing effects is that the resistance of the arc decreases proportionally to $A^{-2/5}$ instead of A^{-1}.

Examples of arc electrical conductivity in SF_6 as a function of time are plotted in Fig. 8 for $F_{SB} = 0.18$, 0.41, and 1.17. The plateau resistances for the arcs are 0.31, 0.27, and 0.20 Ω, respectively. These conductivities, computed from

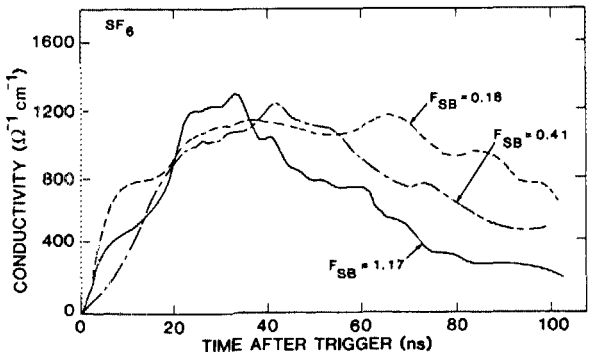

FIG. 8. Electrical conductivity of laser preionization triggered arcs in SF_6 as a function of time after triggering for different values of F_{SB}. The conductivity reaches a maximum value and decreases in spite of the total resistance of the arc monotonically decreasing.

the experimentally derived arc resistances and arc diameters, have a maximum value. The conductivity for arcs operating with large F_{SB} tend to maximize earlier in time than do arcs operating with small F_{SB}. This results from the faster rate of arc expansion obtained with large F_{SB}. Note that when the plateau values of resistance are reached ($t > 50$ ns), the arcs having the largest resistance also have the largest conductivity and, therefore, have the highest temperature.[14] Assuming Spitzer conductivity, the electron temperatures at $t = 100$ ns for the arcs plotted in Fig. 8 are 4.7 eV ($F_{SB} = 0.18$), 3.8 eV ($F_{SB} = 0.41$), and 2.7 eV ($F_{SB} = 1.17$).

The resistances predicted using Eq. (6) for the conditions of the three examples appearing in Fig. 5 are plotted as a function of time in Fig. 9. For these results, $\alpha = 0$ in Eqs. (5) and (6), and they are drawn as the dashed lines in the figure. (The case for $\alpha = 1$ appearing as the solid lines in Fig. 9 will be discussed below.) The predicted values were normalized to the experimental results in Fig. 5 by a multiplicative factor at a single point ($F_{SB} = 1.06$, $t = 90$ ns). Experimental current traces were used for input to the model in each case. The qualitative agreement for this simple theory with the experimental results in Fig. 5 is good. The plateau behavior for resistance is reproduced. The value of the plateau resistance, though, is overpredicted for large values of F_{SB}.

In order for the simple theory described above to obtain better agreement with experiment, the resistance of arcs operating at low F_{SB} must decrease as compared to arcs operating at high F_{SB}. This objective is met by setting the parameter $\alpha = 1$ in Eqs. (5) and (6). Doing so, we obtain the results indicated by the solid lines in Fig. 9. Compare these results to the experimental values plotted in Fig. 5 to see that the agreement with experiment for $\alpha = 1$ is very good.

The physical significance of the parameter α as it appears in the expression for number density, $N(t) \propto F_{SB}^{\alpha} P_0 / A(t)$, is that arcs operating at higher F_{SB} start with a larger diameter. By starting with a larger diameter, more mass is entrained into the arc, thereby decreasing the heating rate per atom. This initial diameter is defined as the diameter of the ionized column at the onset of convective expansion. The initial diameter is determined by the diameter of the laser preionized column and the rate of electron avalanche and photoionization at the edge of the arc. This nonconvective arc expansion was examined with a plasma kinetics and radiation transport model[11] and was found to be important only early during the current pulse ($t < 10$ ns) when the voltage drop across the column is still large. The nonconvective arc expansion was also found to be proportional to $(E/N)_0$ (initial voltage divided by initial number density) at the time of laser triggering.[11] Since large F_{SB} is proportional to $(E/N)_0$, the rate of nonconvective expansion at early times, and hence A_0, will increase with increasing F_{SB}.

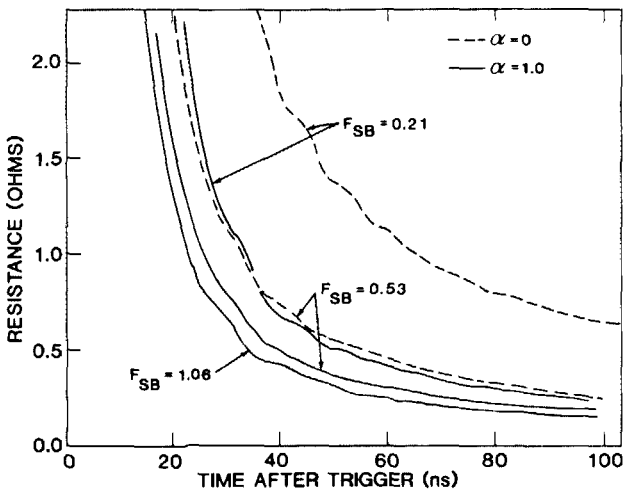

FIG. 9. Theoretical results [see text and Eq. (6)] for the resistance of laser preionization triggered arcs in SF_6 for the conditions of Fig. 5. Results for two different values of the parameter α are plotted. The results for $F_{SB} = 1.06$ are the same for both values of α.

Plateau resistances for laser triggered sparks in SF_6 as a function of F_{SB} are plotted in Fig. 6. The arc resistance decreases with increasing F_{SB} for small values of F_{SB}. At approximately $F_{SB} = 0.8$, the slope of arc resistance vs F_{SB} decreases, and the resistance obtains a relatively constant value. The results of our simple theory, with $\alpha = 1$, are also plotted in Fig. 6 and show good agreement. Two assumptions used in the model, that the mass entrained within the arc is a constant and that the initial arc diameter increases with increasing F_{SB}, appear to be validated by the agreement shown with experiment.

In review, for otherwise fixed conditions, operating at higher F_{SB} implies a faster rate of expansion. A faster rate of expansion decreases resistance by increasing the cross-section area of the arc, while increasing resistance by lowering the electron temperature. Large F_{SB}, though, implies that the initial column diameter is large, thereby decreasing conductivity by increasing the mass entrained in the arc. As indicated, the resistance of the arc as a function of F_{SB} is a convolution of opposing effects. When the resistance of an arc reaches its plateau value, these opposing effects are in balance.

We have observed that the voltage drop across the spark column is large (a few kilovolts/cm) and resistance of the spark column high (a few tenths of an ohm/cm) at the termination of the 100-ns current pulse. These observations are consistent with similar measurements during the first 100 ns of conduction for spark columns of longer duration.[7]

B. Laser-preionization-triggered sparks in other gas mixtures

Arc resistances for sparks in an SF_6/N_2 : 0.3/0.7 gas mixture are plotted in Fig. 10 as a function of F_{SB}. These resistances as a function of F_{SB} are very similar to those measured for pure SF_6 mixtures. They differ in that an asymptotic value does not appear to be reached at high values of F_{SB} for the SF_6/N_2 mixture. When plotted as a function of charging voltage on the PFL at time of triggering (upper scale in Figs. 6 and 10), the lighter gas mixture has a resistance approximately 10% below that of SF_6.

The average molecular weight of the gas mixture through which the arc is sustained impacts the resistance of the arc by two mechanisms. First, since the expansion of the arc is dominantly by hydrodynamic expansion of the ionized core,[8–11] lighter gas mixtures will expand at a faster rate.

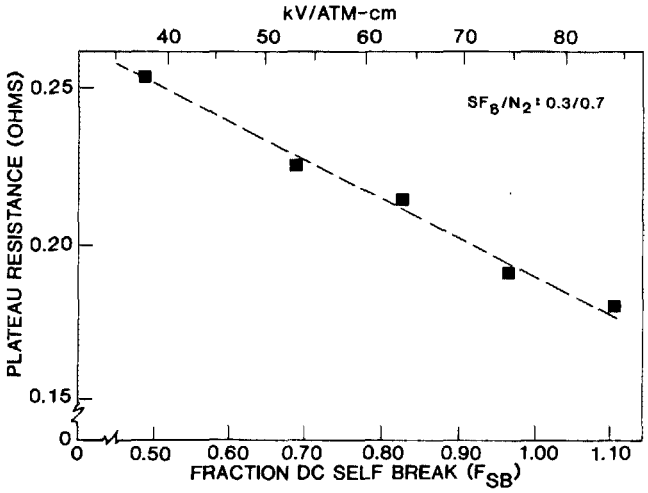

FIG. 10. Plateau arc resistance for lsaer preionization triggered arcs in an SF_6/N_2 : 0.3/0.7 gas mixture as a function of F_{SB}. The equivalent voltage scale is shown at the top of the figure.

(Recall that the sound speed $c_s \propto 1/M^{0.5}$, where M is the average molecular weight of the gas mixture.) For otherwise fixed conditions, arcs with a larger cross-section area will have a lower resistance. The second mechanism is that for equal rates of joule heating, lighter gas mixtures will reach a higher temperature and, therefore, a higher conductivity and a lower resistance. To reduce the resistance of switches, one is motivated to operate with gases having lower molecular weights.

Arc resistance, switch loss (i.e., energy dissipated as joule heating in the spark column), and switching time are plotted in Fig. 11 as a function of average molecular weight for the gas mixtures listed in Table I. The fraction of self-break for each gas mixture is approximately 1.0 ($0.9 < F_{SB} < 1.10$). The switching time is the time after triggering required for the resistance to reach its plateau value. The switch loss was calculated by integrating the product of $[I(t)]^2 R_s(t)$ for 100 ns after triggering. Plateau arc resistance clearly decreases with decreasing molecular weight, as does the switch loss and the switching time. These results indicate

TABLE I. dc self-breakdown voltage coefficients (V_{SB}).

Gas mixture	V_{SB} (kV atm^{-1} cm^{-1})
Xe/H_2 : 0.01/0.99	16.7
CH_4/H_2 : 0.2/0.8	18.2
$SF_6/N_2/He$: 0.05/0.20/0.75	25.0
SF_6/N_2 : 0.3/0.7	76.9
SF_6	108.3

that for the gases investigated, mixtures with smaller average molecular weights should be used for fast, low-loss switches. The caveat, though, is that the self-breakdown voltage coefficient also decreases with decreasing average molecular weight for our mixtures (see Table I). Applications requiring higher holdoff voltages may require a heavier gas mixture (i.e., a mixture with an increasing fraction of SF_6) and, therefore, will have higher switch losses.

The results in Fig. 11 and Table I can be combined for a specified holdoff voltage V_H to yield the minimum permissible average molecular weight and hence the minimum switch loss. To do so, we stipulate that to minimize switch loss, one desires to operate at the maximum fraction of dc self-break for which reliable switching can be obtained. In practice, this value is $F_{SB} \approx 0.75$–0.8. For this exercise, though, we will use $F_{SB} = 1.0$ since our most reliable data is for this value. The systematic trends demonstrated by this optimization will change little for the small difference cited in F_{SB}. We also assume that the switch holdoff voltage is linear with pressure P and with electrode spacing D. The range of molecular weights of interest is 2 amu (hydrogen) to 146 amu (SF_6). The minimum permissable molecular weight, from Table I, is given approximately by

$$M_{opt} \approx 1.5 \frac{V_H}{PD} - 27 \quad \text{amu}, \tag{7}$$

where V_H has units of kilovolts and PD has units of atm cm. To obtain switch loss as a function of M we use the results from Fig. 11. The results plotted in Fig. 11, though, were not obtained at constant pressure, a parameter which appears in

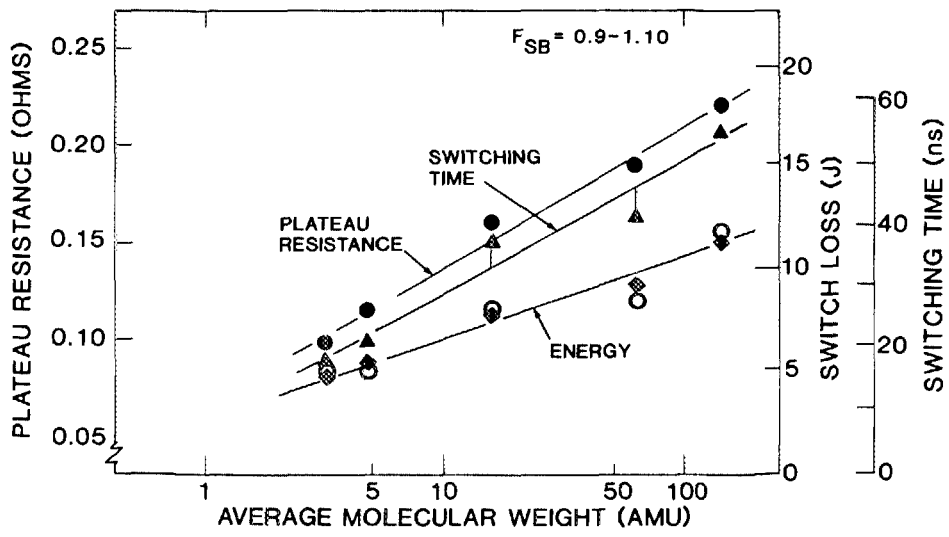

FIG. 11. Plateau arc resistance, switch loss (energy dissipated in the arc), and switching time for laser preionization triggered arcs through the gas mixtures listed in Table I plotted as a function of the average molecular weight of the gas mixture. The fraction of dc self-break that the waterline is charged to is approximately $F_{SB} = 1$ for all cases. The open circles for switch loss were obtained with Eq. (8) ($L = 1.2$ cm).

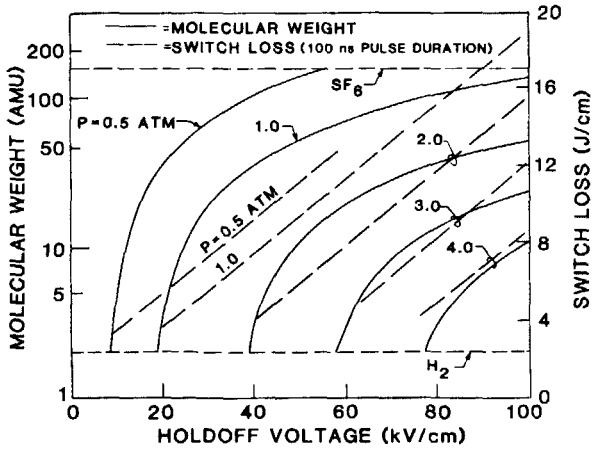

FIG. 12. Minimum switch loss and corresponding molecular weight of the gas mixture as a function of holdoff voltage. Molecular weight and switch loss were obtained from Eqs. (7) and (8).

Eq. (7). In general, pressure decreases with increasing molecular weight in Fig. 11. When pressure is included in the functional dependance of switch loss E_l on M, we find that the product PM (atm amu) is a good scaling parameter. Using this scaling parameter we find that the minimum switch loss is

$$E_l \approx 3.3 + 0.13 PM_{\text{opt}} \text{ J/cm}. \quad (8)$$

This relationship for switch loss is plotted as the open circles in Fig. 11. The minimum switch loss and molecular weight computed with Eqs. (7) and (8) are plotted in Fig. 12 as a function of V_H (kV/cm) for different pressures. Recall that these results are for a 100-ns current pulse duration and a 1.5-Ω PFL. For a given V_H, intersection with a curve of constant P indicates the minimum permissable molecular weight and the minimum switch loss. Switch loss can in general be lowered by operating at a higher pressure of a gas with a lower molecualr weight.

IV. CONCLUDING REMARKS

Arc resistances for a laser preionization triggered spark gap switching a 1.5-Ω, 100-ns pulse-forming line (PFL) have been calculated from measurements using a low inductance capacitive voltage probe, a current-viewing resistor, and a laser interferometer to determine the diameter of the arc. We found that arc resistance during the 100-ns current pulse falls to a plateau value that remains in excess of 0.1 Ω for a variety of gas mixtures. For current pulses of 12–15 kA, the voltage drop across the arc operating through a single channel is in excess of 2 kV. The plateau value of resistance decreases for increasing charging voltage on the PFL at the time of triggering and decreases for decreasing average molecular weight of the gas mixture. The switching time and energy dissipated in the arc also decrease with decreasing average molecular weight of the gas mixture. This dependence on molecular weight results from the fact that the arc expands primarily by hydrodynamic motion of the hot ionized core; lighter gases expand at a faster rate and therefore have a larger cross-section area at a given time after triggering. The optimum switching gas for a particular application is the lightest gas that has the required holdoff voltage. Mixtures of small amounts of SF_6 with light noble gases appear to have the desired characteristics for fast, low-loss spark gaps.

ACKNOWLEDGMENTS

The authors wish to thank Dr. E.A. Crawford at Spectra Technology, Inc. (STI), and Dr. R. J. Gripshover, Dr. E. D. Ball, and Dr. D. B. Fenneman at the Naval Surface Weapons Center for their helpful input during these measurements. The authors also wish to acknowledge D. M. Barrett of STI, who designed the pulsed power system for the experiment, and J.F. Seamans and D. H. Ford of STI for their assistance during the experiment. This work was supported by the Naval Surface Weapons Center under Contract No. N60921-83-C-4057.

[1] J. R. Woodworth, C. A. Frost, and T. A. Green, J. Appl. Phys. **53**, 4734 (1982).
[2] J. R. Woodworth, R. G. Adams, and C. A. Frost, IEEE Trans. Plasma Sci. **PS-10**, 257 (1982).
[3] J. R. Woodworth, P. J. Hargis, Jr., L. C. Pitchford, and R. A. Hamil, J. Appl. Phys. **56**, 1382 (1984).
[4] L. P. Bradley and T. J. Davies, IEEE J. Quantum Electron. **QE-7**, 464 (1971).
[5] A. H. Guenther and J. R. Bettis, J. Phys. D. **11**, 1577 (1978).
[6] R. S. Taylor, A. J. Alcock, and K. I. Leopold, in *Conference Proceedings, IEEE Fourteenth Pulse Power Modulator Symposium, Orlando, FL. (1980)* (IEEE, New York, 1980), p. 32.
[7] J. D. Craggs, in *Electrical Breakdown of Gases*, edited by J. M. Meek and J. D. Craggs (Wiley, Chichester, 1978), p. 753.
[8] W. D. Kimura, E. A. Crawford, M. J. Kushner, and S. R. Byron, in *Conference Record of 1984 Sixteenth Power Modulator Symposium, Arlington, VA* (IEEE, New York, 1984), p. 54.
[9] S. I. Braginskii, Zh. Eksp. Teor. Fiz. **34**, 1548 (1958) [Sov. Phys.—JETP **34**, 1068 (1958)].
[10] M. M. Kekez and P. Savic, in *Electrical Breakdown and Discharges in Gases*, edited by E. E. Kunhardt and L. H. Luessen (Plenum, New York, 1983), p. 419.
[11] M. J. Kushner and R. D. Milroy, in *Conference Record, 1984 IEEE International Conference on Plasma Science, St. Louis, MO* (IEEE, New York, 1984), p. 30.; M. J. Kushner, R. D. Milroy, and W. D. Kimura, J. Appl. Phys. (in press).
[12] D. M. Barrett, S. R. Byron, E. A. Crawford, D. H. Ford, and W. D. Kimura, 1985 High Voltage Workshop, Monterey, CA (unpublished).
[13] D. M. Barrett, S. R. Byron, E. A. Crawford, D. H. Ford, W. D. Kimura, and M. J. Kushner, submitted to Rev. Sci. Instrum.
[14] M. Mitchner and C. H. Kruger, *Partially Ionized Plasma* (Wiley-Interscience, New York, 1973), p. 99.